Proceedings of the IASS Annual Symposium 2019 – Structural Membranes 2019
Form and Force
7 – 10 October 2019, Barcelona, Spain
C. Lázaro, K.-U. Bletzinger, E. Oñate (eds.)

Optimization of tensegrity lattice with truncated octahedral units

Makoto OHSAKI*[a], Jingyao ZHANG[a], Kosuke KOGISO[a], Julian J. RIMOLI[c]

*[a]Department of Architecture and Architectural Engineering, Kyoto University
Kyoto-Daigaku Katsura, Nishikyo, Kyoto 615-8540, Japan
ohsaki@archi.kyoto-u.ac.jp
[b] School of Aerospace Engineering, Georgia Institute of Technology, Atlanta, GA 30332, USA

Abstract

An optimization method is presented for tensegrity lattices composed of eight truncated octahedral units. The stored strain energy under specified forced vertical displacement is maximized under constraint on the structural material volume. The nonlinear behavior of bars allowing buckling is modeled as a bi-linear elastic material. As a result of optimization, a flexible structure with degrading vertical stiffness is obtained to be applicable to an energy absorption device or a vertical isolation system.

Keywords: tensegrity, optimization, strain energy, truncated octahedral unit

1. Introduction

Tensegrity structures are a class of self-standing pin jointed structures consisting of thin bars (struts) and cables stiffened by applying prestresses to their members [1, 3]. Because the bars are not continuously connected, i.e., they are topologically isolated from each other, these structures are usually too flexible to be used as load-resisting components of structures in mechanical and civil engineering applications. However, by exploiting their flexibility, tensegrity structures can be utilized as devices for reducing impact forces, isolating dynamic forces, and absorbing energy, to name a few applications [5]. Lattice structures consisting of tensegrity units are extensively studied to construct a flexible large-scale structure [7, 8]. Wave-propagation properties are also studied [6, 9].

In this study, an optimization method is presented for a recently introduced tensegrity lattice whose unit cell consists of eight truncated octahedral units with threefold symmetry [5]. The objective function to be maximized is the strain energy under specified forced vertical displacement. It is demonstrated in the numerical examples that a stiff structure with degrading tangent stiffness is obtained by maximizing the strain energy. We also show that, for cases where instabilities are present, adding horizontal bars effectively stabilizes the structure.

The remainder of the paper is organized as follow. In Sections 2 and 3 we introduce the basic properties and the configurations of the structure to be studied. In Section 4 we formulate the optimization problem, followed by numerical case studies in Section 5. The conclusions of this work are laid out in section 6.

2. Basic properties of truncated octahedral tensegrity structure

Consider a regular truncated octahedral tensegrity structure as shown in Fig 1(c). The vertices of the octahedron in Fig. 1(a) is removed to generate the truncated octahedron in Fig. 1(b). The members of the tensegrity structure consist of cables and bars, which have tensile and compressive forces, respectively. The cables of the truncated octahedral tensegrity are classified into the edge cables lying on the original edges of the truncated octahedron and the cutting cables lying on its cut edges. The bars are located inside of the truncated octahedron. Hence, a regular truncated octahedral tensegrity structure consists of 24 nodes, 12 bars, 24 cutting cables, and 12 edge cables.

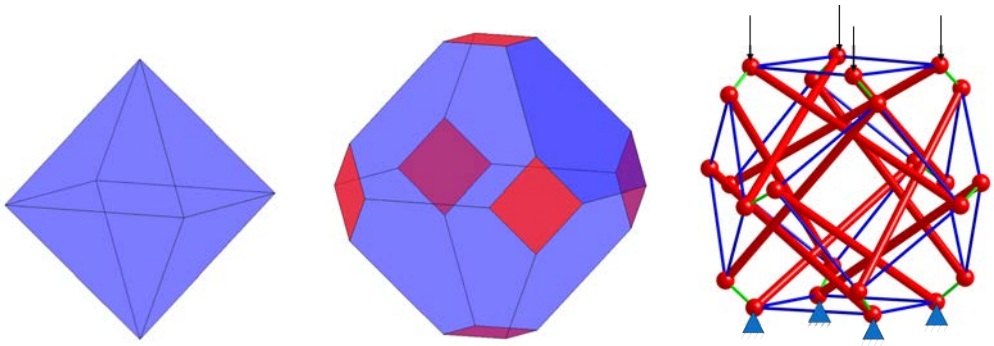

(a) (b) (c)

Figure 1: Generation of regular truncated octahedral tensegrity structure; (a) regular octahedron, (b) truncated octahedron, (c) truncated octahedral tensegrity.

Due to symmetry of the structure, members in each of three types have the same length, and have the same prestress, and accordingly, have the same force density, which is defined as the axial force divided by the member length. Denote the force densities of the edge cables, cutting cables, and bars as q_{e}, q_{c}, and q_{b}, respectively. Define a and b as

$$a = \frac{q_{\mathrm{e}} + q_{\mathrm{b}}}{2}, \quad b = \frac{q_{\mathrm{e}} - q_{\mathrm{b}}}{2} \tag{1}$$

where $b > 0$ is to be satisfied. For the self-equilibrium of a tensegrity structure in 3-dimensional space, its force density matrix necessarily has four zero eigenvalues [1, 3]. From this non-degeneracy condition, we have the force density q_{c} of cutting cables solved as follows [2]:

$$q_{\mathrm{c}} = \frac{b^2 - 5a^2 + \sqrt{a^4 + 14a^2b^2 + b^4}}{4a} \tag{2}$$

for which we need $a > 0$ for proper signs for the force densities as well as *super-stability* of the resulting structure. The scaling parameter β is used to adjust the level of force densities as $\beta\mathbf{q}$. Since the force density matrix is also scaled by β at the same time, the self-equilibrium equations remain to be satisfied by the same configuration.

It is known that a regular truncated octahedral tensegrity has only one mode of prestress and 19 infinitesimal mechanisms. Furthermore, this structure is known to be *super-stable* when $q_{\mathrm{e}} = 1.0$ and $-1 < q_{\mathrm{b}} < 0$, which means that it is always stable irrespective of material properties as well as level of prestress [4], if yielding of cables and buckling of bars are not considered.

Eight units of regular truncated octahedral tensegrity structures are combined to obtain the tensegrity lattice as shown in Fig. 2. The units are combined symmetrically with respect to the horizontal plane and the two vertical planes. The four nodes of each truncating section are connected to those of another unit, where one of the duplicate cables at each connection is removed. Hence, the number of members is 336, and the number of nodes is 96 in this eight-unit tensegrity lattice.

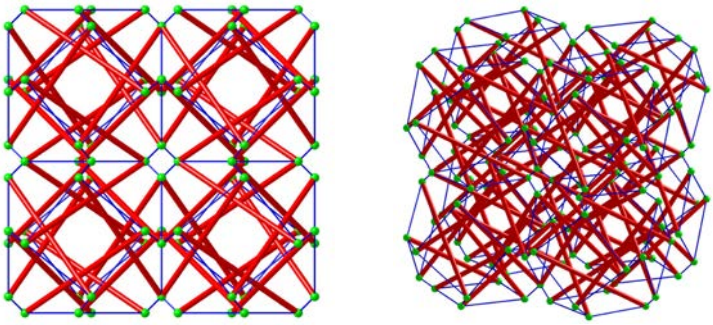

(a) (b)

Figure 2: Undeformed shape of eight-unit tensegrity lattice; (a) plan/elevation, (b) diagonal view.

3. Large-deformation analysis under forced vertical displacement

In this work, a large-deformation analysis and optimization is carried out for the eight-unit tensegrity lattice in Fig. 2. For more details about the generation of this structures and its fundamental mechanical properties we refer the reader to reference [5]. Let l_0 and l denote the length of a member before and after deformation, respectively, under axial force f. We are particularly interested in the deformation regime for which bars undergo buckling. A bilinear elastic model is used for representing buckling behavior of a bar. The relation between compressive axial force $|f|$ and axial contraction $|\Delta l| = |l - l_0|$ of a bar is shown in Fig. 3, where f_b is the Euler buckling load. Stiffness EA of the bar is zero after buckling. When the member is in prebuckling range, its strain energy is calculated from

$$S = \frac{EA}{2l_0}(l - l_0)^2 \tag{3}$$

After buckling, its strain energy is obtained as

$$S = \frac{f_b^2 l_0}{2EA} + f_b \left| l - l_0 - \frac{f_b l_0}{EA} \right| \tag{4}$$

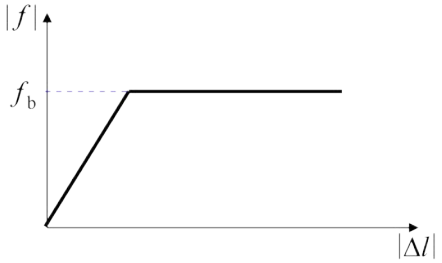

Figure 3: Bilinear elastic buckling model between compressive axial force $|f|$ and contraction $|\Delta l|$ of a bar.

The Euler buckling stress for the bars is computed from the slenderness ratio, and tension in bars is allowed. The yield stress of cables is assumed to be sufficiently large so that cables remain in elastic range, and its strain energy is computed from Eq. (3). Slackening of cable is checked after obtaining the optimal solution. Tangent stiffness matrix is derived as the sum of linear stiffness matrix and geometrical stiffness matrix. Forced displacement is applied incrementally, and unbalanced forces are reduced using Newton iteration at each step.

4. Formulation of optimization problem

Let L_b and L_c denote the total lengths of bars and cables, respectively. The cross-sectional areas of bars and cables are denoted by A_b and A_c, respectively, which are chosen as design variables. Objective function is the strain energy S stored before reaching the specified vertical displacement at the top layer. Here, for simplicity, the strain due to initial prestress is included in evaluation of the total strain energy. The constraints are given as follows so that the total structural volume does not change from the initial volume V_0:

$$A_b L_b + A_c L_c = V_0 \tag{5}$$

Another variable is β denoting the scaling parameter representing level of prestress that is multiplied to forces of all cables and struts at the initial undeformed state. The force density q_b (<0) of bars is considered as a parameter to obtain optimal solutions of various shapes, while the force density of the edge cables is fixed at $q_e = 1.0$. Note again that the shape is determined by the force density only; therefore, the undeformed shape does not change during the optimization process. A small value is assigned for the radius of gyration of the section so that Euler buckling precedes the yielding of a bar.

The optimization problem for finding A_b, A_c, and β for maximizing the total strain energy $S(A_b, A_c, \beta)$ is formulated as

$$\begin{aligned} &\text{Maximize } S^*(A_b, A_c, \beta) \\ &\text{sunject to } A_b L_b + A_c L_c = V_0 \\ &\qquad A_b^L \le A_b \le A_b^U,\ A_c^L \le A_c \le A_c^U \\ &\qquad \beta^L \le \beta \le \beta^U \end{aligned} \tag{6}$$

where the superscripts ‘U’ and ‘L’ are the upper and lower bounds of the variables.

5. Numerical examples

We optimized an eight-unit tensegrity lattice as shown in Fig. 2. The members are assumed to be made of steel material with Young's modulus $E = 2.05\times10^5$ N/mm^2. Let the *nominal volume* of the structure denote the volume of the cuboid in which the structure is inscribed. The volume of the surrounding cuboid is $8\times0.004 = 0.032$ m^3; i.e., shape of the structure is scaled to have the nominal volume of 0.032 m^3 for each configuration defined by q_b. Since length of the bar is about 170 mm, the radius of gyration is assumed to be 1.2 mm so that elastic buckling occurs before yielding.

In the bottom plane, the *z*-directional displacement is constrained at all nodes, *x*- and *y*-directional displacements are constrained at a node, and *x*- or *y*-directional displacement is constrained respectively at two of the remaining nodes. This way, rigid-body displacements and rotations are constrained allowing expansion of the bottom square. On the other hand, the 16 nodes in the top layer are enforced to move 80 mm in negative *z*-direction constraining rigid-body displacement and rotation in the similar manner as the bottom plane. The deformation is computed using displacement increment method with 1.0 mm at each step. A small stiffness *EA*/100 is assigned for a bar after buckling to stabilize the process.

As noted in Sec. 2, each truncated octahedral unit is super-stable when $-1 < q_b < 0$ while q_e is fixed at. Therefore, the parameter q_b is varied as –0.3, –0.4, –0.5, –0.6, and –0.7. The lower and upper bounds for the cross-sectional areas are 0.1 mm^2 and 10.0 mm^2, respectively, for all members including cables and bars. The specified total volume of members is 2.2687×10^3 mm^3. The lower and upper bounds of the stress level β are 0.2 and 20.0, respectively. The optimization problem is solved using sequential

quadratic programming available in the function *fmincon* of the optimization toolbox of MATLAB Ver. 2018.

Table 1: Optimization results.

q_b	A_s (mm^2)	A_c (mm^2)	β	S (Nm)
–0.3	0.9179	0.1000	1.6536	9601
–0.4	0.9806	0.1000	1.7617	10130
–0.5	1.0456	0.1000	1.9449	14185
–0.6	1.1106	0.1000	1.9451	23137
–0.7	1.1742	0.1000	1.8395	37734

Optimal solutions as well as the optimal objective values are listed in Table 1 for various values of q_b. The cable cross-sectional area has its lower-bound value for all cases, and the cross-sectional area of bars and the objective function value increase as q_b is decreased. The stress level β mostly increases as q_b is decreased. The deformed shapes of optimal solutions are shown in Fig. 4. As seen from the figure, the length of strut decreases as q_b is decreased; accordingly, the squares at the truncated vertices become smaller and the initial stiffness increases.

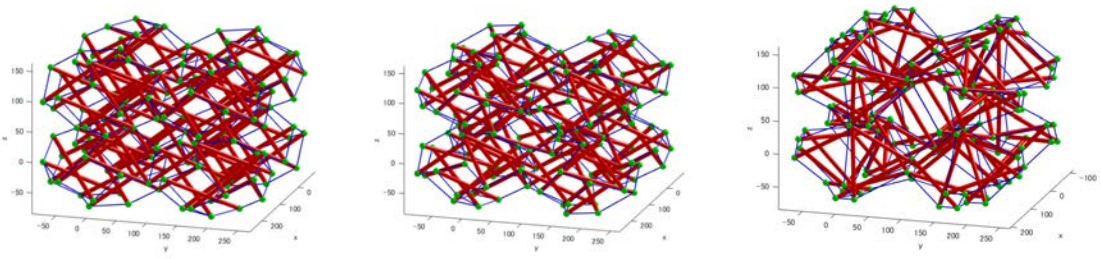

(a) $q_b = -0.3$ (b) $q_b = -0.5$ (c) $q_b = -0.7$

Figure 4: Deformed shape of optimal solutions.

Relation between the vertical downward displacement of top nodes and the sum of vertical reaction forces at all top nodes are plotted in Fig. 5. As seen from the figure, the vertical stiffness decreases as the downward displacement is increased. Furthermore, the maximum reaction force increases as q_b is decreased. The structure has a limit point instability for $q_b = -0.7$; i.e., it has a snap-through behavior if the deformation is controlled by the vertical load instead of the vertical displacement.

The member forces are plotted with respect to the vertical displacement in Fig. 6. Note that the axial force has positive value in tensile state. Although we do not consider slackening or yielding of cables, the cable forces have non-smooth distributions, which is caused by buckling of bars. It is seen from the results that the number of buckled members increases as vertical displacement is increased.

Although the optimal structures have positive vertical stiffness except for the case of $q_b = -0.7$, horizontal stiffness may be lost when q_b is small due to shear deformation of the upper and lower units. To prevent instability in horizontal direction, additional bars are attached as shown in Fig. 7 in one or two of the top, bottom, and middle layers of the lattice. Optimization is carried out for $q_b = -0.7$ and –0.8, because a smaller value of q_b is effective to have more strain energy.

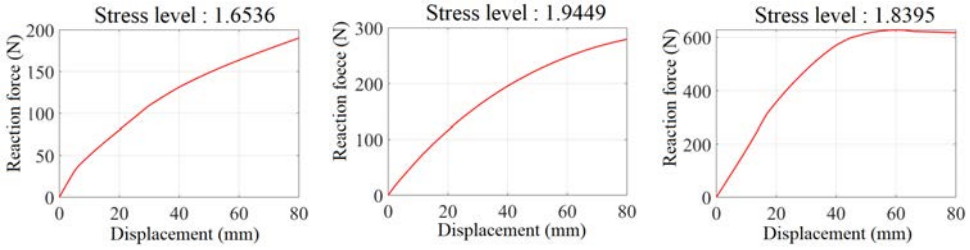

(a) $q_b = -0.3$ (b) $q_b = -0.5$ (c) $q_b = -0.7$

Figure 5: Relation between vertical displacement and reaction force.

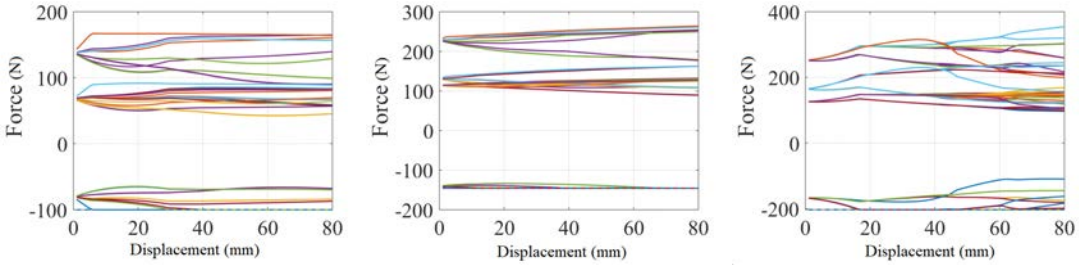

(a) $q_b = -0.3$ (b) $q_b = -0.5$ (c) $q_b = -0.7$

Figure 6: Relations between vertical displacement and member forces.

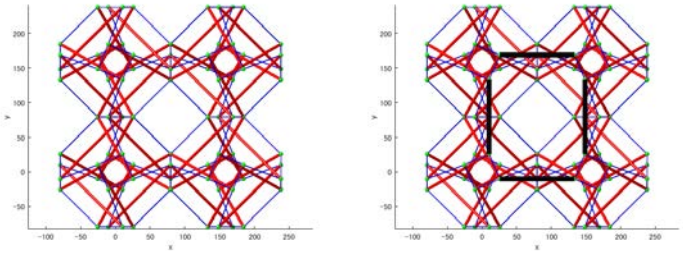

(a) (b)

Figure 7: Additional bars in eight-unit lattice; (a) without bars, (b) with four additional bars.

Table 2: Optimization results of eight-unit lattice with additional four bars in various patterns of layers.

Layers for adding bars	q_b	A_s (mm^2)	A_c (mm^2)	β	S (Nm)
Top	–0.7	1.1294	0.1000	1.8137	38338
	–0.8	1.1825	0.1000	1.8103	38549
Top and middle	–0.7	1.0879	0.1000	1.5261	44891
	–0.8	1.1322	0.1000	1.5060	72591
Top and bottom	–0.7	1.0879	0.1000	1.7596	37265
	–0.8	1.1322	0.1000	1.6076	63305
Top, middle, and bottom	–0.7	1.0493	0.1000	1.3264	62863
Middle	–0.7	1.1294	0.1000	1.8230	38653
	–0.8	1.1825	0.1000	1.6698	66019

Optimization results are listed in Table 2. For example, 'top' means that four bars are added in the top layer. The deformed configuration, force-displacement relation, and load-displacement relation are shown in Fig. 8 for $q_b = -0.7$ with bars in the middle layer.

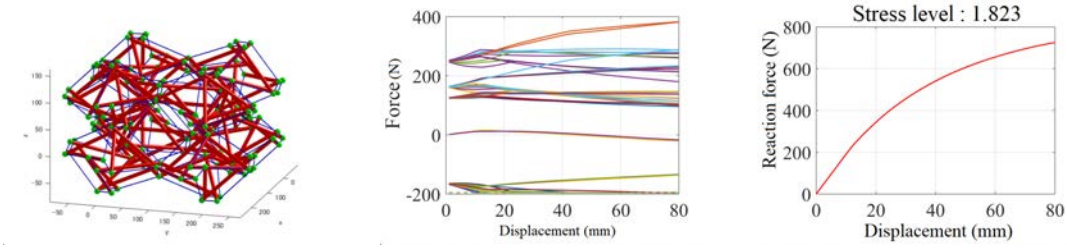

Figure 8: Property under vertical loading of the optimal solution for $q_b = -0.7$ with bars in top and bottom layers; (a) diagonal view of deformed shape, relation between displacement and axial forces, (c) relation between displacement and reaction force..

Shear stiffness in *x*-direction is next investigated after application of vertical displacement of 30 mm. The condition of forced vertical displacement is replaced to application of vertical loads that are equal to the reaction force at the forced displacement of 30 mm.

It was found that the structure is still unstable for the shear deformation, if the support conditions at the bottom layer are not modified. Therefore, all bottom nodes are pin-supported after application of downward displacement of 30 mm. The deformed configuration, histories of member forces, and load-displacement relation are shown in Fig. 8 for $q_b = -0.7$ with bars in the middle layer. The rocking deformation may be suppressed depending on the boundary conditions for practical application as, e.g., base isolation of structures. Suppression of rocking may lead to further stabilization of the structure. It has been confirmed that the vertical load-displacement relation remains almost the same after constraining the nodes in the bottom layer.

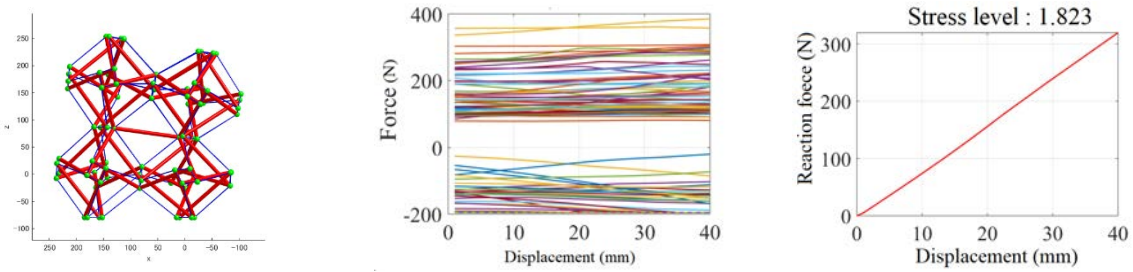

(a) (b) (c)

Figure 9: Property under horizontal loading of the optimal solution for $q_b = -0.7$ with bars in top and bottom layers; (a) elevation of deformed shape, relation between displacement and axial forces, (c) relation between displacement and reaction force.

6. Conclusions

An optimization method has been presented for tensegrity lattices composed of eight truncated octahedral units. The stored strain energy under specified forced vertical displacement is maximized under constraints on the structural material volume. It has been shown in the numerical examples that a flexible structure with degrading vertical stiffness is obtained as a result of optimization. Although structures generally retain compression stiffness even after large deformations, in some cases shear stiffness is lost. This issue can be addressed on those optimal solutions by adding four bars in some of the layers of the lattice. In this way, a tensegrity lattice with flexibility in vertical direction and adequate shear stiffness can be obtained to be applicable to an isolation system for vertical motion.

Acknowledgements

This research is partly supported by SPIRITS program of Kyoto University.

References

[1] J. Y. Zhang and M. Ohsaki, Adaptive force density method for form-finding problem of tensegrity structures, Int. J. Solids and Struct., Vol. 43, No. 18-19, pp. 5658--5673, 2006.

[2] J. Y. Zhang, M. Ohsaki and F. Tsuura, Self-equilibrium and stability of regular truncated hexahedral and octahedral tensegrity structures, *Int. J. Solids Struct*., 2019.

[3] J. Y. Zhang and M. Ohsaki, *Tensegrity Structures: Form, Stability, and Symmetry*, Mathematics for Industry 6, Springer, 2015.

[4] J. Y. Zhang and M. Ohsaki, Stability conditions for tensegrity structures, Int. J. Solids and Struct., Vol. 44, No. 11-12, pp. 3875-3886, 2007.

[5] J. J. Rimoli and R. K. Pal, Mechanical response of 3-dimensional tensegrity lattices, *Composites Part B*, Vol. 115, pp. 30–42, 2017.

[6] J. J. Rimoli, A reduced-order model for the dynamic and post-buckling behavior of tensegrity structures, *Mechanics of Materials*, Vol. 116, pp. 146–157, 2018.

[7] L.-Y. Zhang *et al*., Automatically assembled large-scale tensegrities by truncated regular polyhedral and prismatic elementary cells, Composite Structures, Vol. 184, pp. 30-40, 2018.

[8] X.-Q. Feng *et al*., Design methods of rhombic tensegrity structures, Acta Mech. Sin., Vol. 26, pp. 559-565, 2010.

[9] F. Fabbrocino and G. Carpentieri, Three-dimensional modeling of the wave dynamics of tensegrity lattices, Composite Structures, Vol. 173, pp. 9-16, 2017.